Combined Spectroelectrochemical and Theoretical Study of a Vinylene-Bridged Sexithiophene Cooligomer: Analysis of the π-Electron Delocalization and of the Electronic Defects Generated upon Doping

J. Casado,[†,‡] L. L. Miller,*[,†] K. R. Mann,[†] T. M. Pappenfus,[†] Y. Kanemitsu,[§] E. Ortí,*[,||] P. M. Viruela,[||] R. Pou-Amérigo,[||] V. Hernández,[‡] and J. T. López Navarrete*[,‡]

Department of Chemistry, University of Minnesota, Minneapolis, Minnesota 55455, Graduate School of Materials Science, Nara Institute of Science and Technology, Takayama, Ikoma, Nara, 630-01, Japan, Institut de Ciència Molecular, Universitat de València, 46100-Burjassot (Valencia), Spain, and Departamento de Química Física, Facultad de Ciencias, Universidad de Málaga, 29071-Málaga, Spain

Received: December 13, 2001

The electronic and the Fourier transform Raman (FT-Raman) spectra of a novel well−barrier−well vinylene-bridged sexithiophene in neutral and in doped states have been recorded. The samples were oxidized chemically, with trifluoroacetic acid or ferric chloride, and electrochemically in dichloromethane solutions. The evolution of the Raman spectral pattern upon oxidation at different anodic potentials has been analyzed for a thin solid film of the material. Experimental observations are explained by the initial generation of a radical cation species followed by the generation of a dication species. A comprehensive assignment of the electronic and Raman spectroscopic features observed in both neutral and oxidized states has been performed on the basis of density functional theory (DFT) calculations. Time-dependent DFT calculations have been performed to calculate the electronic excitation energies. The experimental data and theoretical results give a clear picture of the structure and electronic properties of the charge defects created on this vinylene-bridged sexithiophene.

I. Introduction

Low band-gap π-conjugated polymers are the subject of an intense research effort as functional materials for a variety of electronic and photonic applications.[1] However, a number of characteristics (polydispersity, low crystallinity and solubility, chemical defects, etc.) present in polymeric materials have made it difficult to establish a precise structure/electronic properties relationship. So this represents a serious shortcoming in developing applications that require a more strict control of the structural and electronic properties. To avoid these problems, a large variety of π-conjugated oligomers with perfectly controlled chemical structures have been investigated over the past decade.[2−4] Monodisperse conjugated oligomers are very useful as model compounds for elucidating the electronic properties of the parent polymers. They have also gained interest in their own right as a novel class of molecular materials investigated as organic semiconductors for the fabrication of electronic and optoelectronic devices. The control of their chemical structure and electronic properties is therefore the focus of considerable current interest.[5,6] Their possible use as molecular wires in molecular electronics or nanoscopic systems has recently attracted special attention.[7,8]

Among conjugated oligomers, oligothiophenes have been extensively studied in the past few years.[9] The sexithiophene oligomer has been used as an active component in electronic devices such as field effect transistors (FET) and light emitting diodes (LED).[10,11] In the case of electroluminescent devices, certain electronic requirements in terms of charge and energy transport as well as photon emission must be fulfilled. In this sense, nonhomogeneous oligomers or cooligomers (built up from different conjugated units such as benzene, pyrrole, thiophene, or vinylene) have been synthesized. These new systems, in some specific cases, show improved electroluminescent properties compared to homogeneous oligothiophenes. For example, lower band-gap molecules with enhanced intramolecular charge-transfer excitations are obtained.[12,13]

Electronic and Raman spectroscopies have been used as complementary techniques to study π-conjugated polymers and oligomers, which show strong electron−phonon coupling due to their quasi one-dimensional structures. Raman spectroscopy has been shown to be a particularly powerful tool in estimating the extent of conjugation in neutral systems and in characterizing conjugational defects in doped π-conjugated materials.[14−17] On the basis of the effective conjugation coordinate (ECC) theory,[18,19] the appearance of a few Raman bands for linear π-conjugated systems is directly related to the extent of the electron−phonon coupling (electronic delocalization) over the molecular domain. The ECC theory states that when the conjugation length (CL) increases, the bands involved in the ECC mode downshift in frequency. The frequency downshift recorded for these Raman bands as the molecular length increases is very useful in evaluating the CL in a homogeneous series of neutral oligomers. On the other hand, when conjugated oligomers and, in particular, oligothiophenes are oxidized or doped, typically quinonoid structures are created.[20] This structural change also produces a downshift of the frequencies associated to the conjugation path. The evolution of the Raman bands between the neutral and the different doped states is a useful tool for elucidating the type of charge defects created upon oxidation.

[†] University of Minnesota.
[‡] Universidad de Málaga.
[§] Nara Institute of Science and Technology.
[||] Universitat de València.

10.1021/jp0145210 CCC: $22.00
Published on Web 03/23/2002

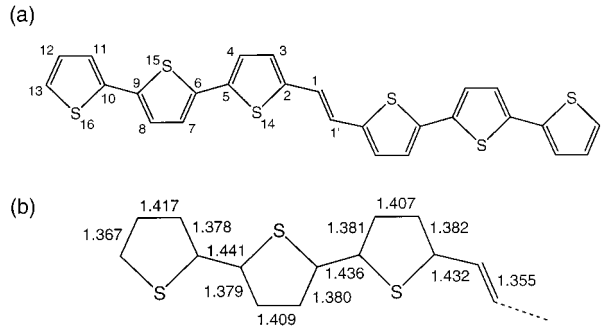

Figure 1. Chemical structure of T3VT3: (a) atom numbering; (b) B3P86/6-31G** optimized bond lengths (in angstroms) for half the molecule (C_{2h} symmetry).

Electrochemical techniques are among the most extended methods to generate and study molecular charged species. The analysis of the cyclic voltammetry (CV) waves is a widely used method to study the electrochemical behavior of conjugated molecules.[21−24] However, these studies must be combined with other techniques to provide a deeper insight on the type, structure, and stability of the charge defects created upon doping. In this sense, a number of papers have been recently published trying to get evidence of the structure and electronic properties of oxidized oligomers and cooligomers using a variety of experimental and theoretical techniques. For instance, van Haare et al. have demonstrated the occurrence of two polarons instead of a bipolaron for dodecathiophene dication on the basis of electrochemical, UV−vis−NIR absorption, and ESR spectroscopy data and quantum chemical calculations.[25] Tol previously proposed the transition between a bipolaron and two isolated polarons, as the energetically favored structure for long oligothiophenes, on the basis of semiempirical calculations.[26]

Some of us have recently reported a vibrational study of a π-conjugated oligomer, T2VT2, consisting of bithienylene (T2) units connected through a vinylene bridge (V).[27] T2VT2 can be visualized as a molecule formed by two end moieties with a lower energy gap than the central vinylene spacer. The radical cation of T2VT2 was also investigated by FT-IR and FT-Raman spectroscopies, but it was not possible to characterize the dication likely due to the short molecular size.[28] The Raman spectrum of the shorter 1,2-bis(thienylene)vinylene (TVT) oligomer in the neutral state has been also reported in the literature.[29]

In this work, we focus on a new thiophene-based cooligomer built up from two α,α'-terthienylene units connected via a vinylene group, T3VT3. FT-Raman and UV−vis−NIR spectroscopies together with density functional theory (DFT) calculations are used to characterize the structure and electronic properties of T3VT3 in both neutral and doped states. Our main goals are to determine the type of charge defects created upon doping and to rationalize their electronic and Raman spectroscopic features.

II. Experimental and Computational Details

The chemical structure of T3VT3 is depicted in Figure 1. The synthesis and purification methods are described elsewhere.[30] Cyclic voltammetry was carried out in a saturated solution of T3VT3 in CH_2Cl_2. Tetrabutylammonium tetrafluoroborate ($TBABF_4$) was used as the supporting electrolyte in 0.1 M concentration. A glassy carbon electrode and a platinum electrode were used as working and as auxiliary electrodes, respectively. All electrochemical measurements were carried out using a Ag/AgCl electrode as the reference electrode.

Chemical oxidations in dichloromethane solutions were carried out with trifluoroacetic acid in the presence of light and oxygen, as previously described,[31] or with ferric chloride. Raman spectroelectrochemical measurements were carried out in thin solid films at room temperature. The films were made by solvent evaporation of a dichloromethane dispersion. The experimental procedure was as follows: the coated platinum electrode was immersed into the 0.1 M $TBABF_4$ dichloromethane solution, and a fixed anodic potential was applied for 60 s. The selective oxidation of the film was performed by choosing the anodic potential on the basis of the cyclic voltammogram previously obtained. In all the experiments, a Voltalab40 electrochemical equipment from Radiometer was employed.

Electronic spectra in the near-IR region were measured with a Nicolet 550 NIR Spectrometer equipped with a PbSe detector. Spectra in the UV−vis region were measured with an Ocean Optics Spectrometer equipped with a Silicon detector. FT-Raman spectra were measured using the FT-Raman accessory kit (FRA/106-S) of a Bruker Equinox 55 FT-IR interferometer. A continuous-wave Nd:YAG laser working at 1064 nm was employed for Raman excitation. A germanium detector operating at liquid nitrogen temperature was used. Raman scattering radiation was collected in a backscattering configuration with a standard spectral resolution of 4 cm^{-1}. To avoid possible damage of the sample upon laser radiation, the laser beam was loosely focused on the sample and its power was kept below 30 mW. In all Raman experiments, one thousand scans were averaged to improve the signal-to-noise ratio.

All the calculations were carried out at the DFT level using the A.7 revision of the GAUSSIAN 98 program package[32] running on SGI Origin 2000 computers and IBM RS/6000 workstations. Geometry optimizations and Raman spectra calculations were performed using the Becke's three-parameter B3P86[33] and B3LYP[34] exchange-correlation functionals together with the 6-31G** basis set.[35] Although the B3LYP functional is more widely used in the literature, the B3P86 functional has been recognized to provide equilibrium geometries for sulfur-containing compounds that are in better accord with gas-phase experimental data and ab initio post-Hartree−Fock (HF) calculations.[36−38] The radical cation and the two-polaron dication of T3VT3 were treated as open-shell systems and were computed using spin-unrestricted DFT wave functions (UB3P86 and UB3LYP).

The calculated harmonic vibrational frequencies were scaled down uniformly by a factor of 0.96, as recommended by Scott and Radom.[39] All quoted vibrational data are thus scaled values. The theoretical Raman spectra were obtained by convoluting the scaled frequencies with Gaussian functions (10 cm^{-1} width at the half-maximum). The height of the Gaussians was determined from the Raman scattering activities calculated for the Raman-active normal modes. The relative intensity of the most intense Raman line appears to be theoretically overestimated by comparison with experimental Raman bands.

Vertical electronic excitation energies were computed by using the time-dependent density functional theory (TDDFT).[40−43] The computational cost of TDDFT is roughly comparable to single excitation theories based on a HF ground state, such as single-excitation configuration interaction (CIS). Numerical applications reported so far indicate that TDDFT employing current exchange-correlation functionals performs significantly better than the HF-based single excitation theories for the low-lying valence excited states of closed-shell[44,45] and open-shell[46] molecules.[47] TDDFT calculations were carried out using the B3P86 functional and the 6-31G** basis set. Calculations using

the more extended 6-311G** basis set[48] were also done for neutral T3VT3.

III. Neutral T3VT3

(a) Molecular Structure. The molecular geometry of T3VT3 was first optimized assuming a planar C_{2h} structure in which terthiophene units are in all-anti arrangements. Two C_{2h} conformations were actually considered. Conformation A corresponds to that depicted in Figure 1a, for which the vinylene C1═C1′ double bond is in an anti disposition with respect to the C2═C3 bonds of the neighboring thiophene rings. In conformation B, the vinylene C═C bond is in a syn disposition. Conformation A was calculated to be more stable than conformation B by 2.74 kcal/mol at the B3P86 level.

Conformation A was reoptimized in a second step under no symmetry restriction, thus relaxing the steric hindrance in the interannular regions. This relaxation leads to a slightly twisted structure, due to rotation around the inter-ring bonds, which is more stable by only 0.18 kcal/mol (at the B3P86 level) and presents dihedral angles of about 5−14°. Conformation A was also calculated at the HF/6-31G** level because DFT calculations have been suggested to overestimate the stability of planar conformers for conjugated molecules.[49,50] HF calculations produce a slightly more twisted structure with torsional angles of about 30°, which is 1.25 kcal/mol lower in energy than the fully planar structure. These small energies suggest that the molecule will adopt a fully planar structure in the solid state, as it has been experimentally observed for sexithiophene.[51]

Figure 1b displays the optimized B3P86/6-31G** bond lengths of the carbon−carbon (CC) bonds forming the conjugation path for the planar A conformation of T3VT3. The shortest bond distance corresponds to the vinylene C1═C1′ double bond (1.355 Å), while the longest distances are those of the C1−C2 bonds connecting the terthiophene units to the vinylene spacer and those of the inter-ring bonds (1.43−1.44 Å). The thiophene rings directly attached to the vinylene bridge present a single−double CC bond alternation of 0.026 Å, which increases to 0.030 Å for the central thiophene rings and to an average value of 0.045 Å for the outer rings. All these trends show that the π-conjugation is more effective in the center of the molecule and weakens on the outermost rings.

B3LYP/6-31G** calculations lead to the same structural trends obtained from B3P86 calculations. The average deviation between the optimized B3LYP CC bond lengths and those reported in Figure 1b is as small as 0.003 Å. The only difference worth mentioning between B3P86 and B3LYP optimized geometries concerns the values calculated for the C−S bond lengths. The B3P86 functional predicts an almost constant value of 1.745 Å, except for the terminal C13−S16 bonds (1.723 Å) due to end-chain effects, while the B3LYP functional provides a longer value of 1.759 Å. As mentioned above, B3P86-optimized bond lengths are closer to gas-phase experimental data for sulfur-containing compounds.[36−38]

(b) Electronic Spectrum. The UV−vis spectrum recorded for neutral T3VT3 in CH_2Cl_2 solution presents an intense absorption band in the visible region centered at 464 nm (2.67 eV). To investigate the electronic transitions that give rise to this band, the lowest-energy electronic excited states of T3VT3 were calculated using the TDDFT approach together with the B3P86 functional and the 6-31G** and 6-311G** basis sets. The geometry optimized at the B3P86/6-31G** level for conformation A (C_{2h}) was used in the TDDFT calculations.

B3P86/6-31G** calculations indicate that the first excited, dipole-allowed electronic state is the $1\ ^1B_u$ state, which is calculated at 2.28 eV above the 1^1A_g ground state. The transition to the ^1B_u state is expected to be very intense since it has a calculated value for the oscillator strength (f) of 2.34. Three other transitions to 1^1B_u states are calculated below 4 eV (3.34, 3.48, and 3.80 eV) but they show smaller oscillator strengths (f = 0.01, 0.21, and 0.09, respectively). The use of the triple-ζ 6-311G** basis set affects the excitation energies by only a few hundredths of an electronvolt.

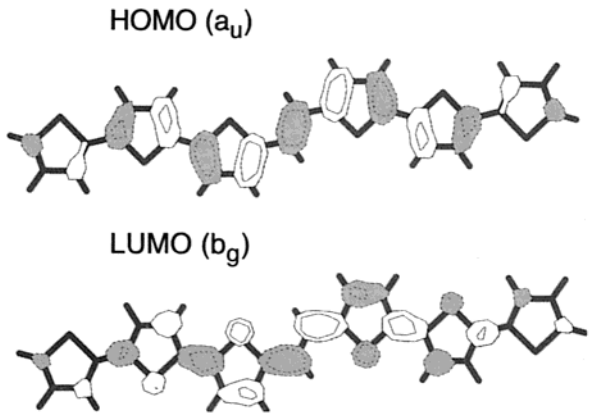

Figure 2. Electronic density contours (0.03 e/bohr^3) calculated for the HOMO and LUMO of T3VT3 at the B3P86/6-31G**.

On the basis of the theoretical results, the intense absorption band observed experimentally for T3VT3 is assigned to the $1^1A_g \rightarrow 1^1B_u$ transition calculated at 2.28 eV. The analysis of the wave function of the 1^1B_u state indicates that this transition corresponds to a one-electron excitation from the HOMO (highest occupied molecular orbital) to the LUMO (lowest unoccupied molecular orbital). The atomic orbital composition of these molecular orbitals is sketched in Figure 2. The HOMO is delocalized along the CC backbone and corresponds to the HOMO of a polyenic chain. The LUMO presents small contributions from the sulfur atoms but basically corresponds to the LUMO of a polyene. The 1^1B_u state of T3VT3 is very similar to the 1^1B_u state in polyenes, which also results from the HOMO → LUMO excitation and gives rise to the intense absorption in the UV−vis spectrum.[52,53] Our assignment is furthermore supported by the comprehensive TDDFT study reported by Hsu et al.[45] for polyenes. These authors show that TDDFT underestimates the excitation energy of the 1^1B_u state by 0.4 eV when hybrid functionals are employed. As for polyenes, the transition to the 1^1B_u state in T3VT3 (2.28 eV) is calculated 0.4 eV lower in energy than the absorption band observed experimentally (2.67 eV).

(c) Raman Spectrum. The Raman spectrum of the neutral form of T3VT3 in the solid state and the previously reported spectrum for T2VT2 are shown in Figure 3.[27] Both spectra show the characteristic features common to many classes of conjugated oligomers:[14−19] (i) only a few Raman lines, in the aromatic C═C stretching region, are experimentally observed despite the complexity of the chemical structures, and (ii) certain Raman bands downshift in frequency from T2VT2 to T3VT3. Table 1 summarizes the frequencies measured in the Raman spectra for T3VT3 and T2VT2,[27] together with those recorded for a series of α,α′-dimethyloligothiophenes (homogeneous oligothiophenes) of variable chain length.[54]

Figure 4 plots the Raman spectrum calculated for T3VT3 at the B3P86/6-31G** level, and Figure 5 sketches the theoretical eigenvectors (atomic vibrational displacements) associated with the most intense Raman bands. The B3LYP functional provides an identical description of the Raman spectrum and the vibrational frequencies afforded by this functional are quoted

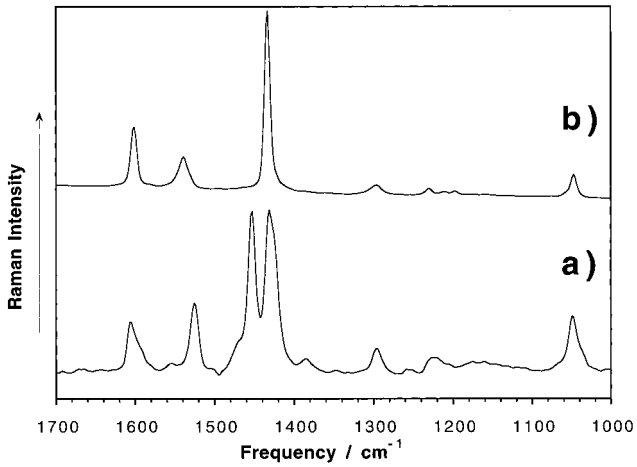

Figure 3. FT-Raman spectra of neutral T3VT3 (a) and T2VT2 (b) in the solid state (spectral range: 1700−1000 cm^{-1}).

TABLE 1: Correlation between the Vibrational Raman Frequencies of the Neutral DMTT, DMQtT, DMQqT, T2VT2, and T3VT3[a]

DMTT[b]	DMQtT[b]	DMQqT[b]	T2VT2[c]	T3VT3
			1601	1606
1561	1564	1562		
				1555
1546	1533	1525	1539	1525
1488	1482	1481		
1476	1469			
1445	1448	1450		1453
			1433	1432
				1420 sh
				1385
1357	1359	1361		
				1347
1288			1296	1296
1258	1261			1258
1229	1224	1219	1230	1225
				1175
1165	1164	1160		1160
1068	1058	1049	1047	1049
1044	1044			

[a] DMTT: α,α′-dimethylterthiophene; DMQtT: α, α′-dimethylquaterthiophene; DMQqT: α,α′-dimethylquinquethiophene. [b] From ref 54. [c] From ref 27.

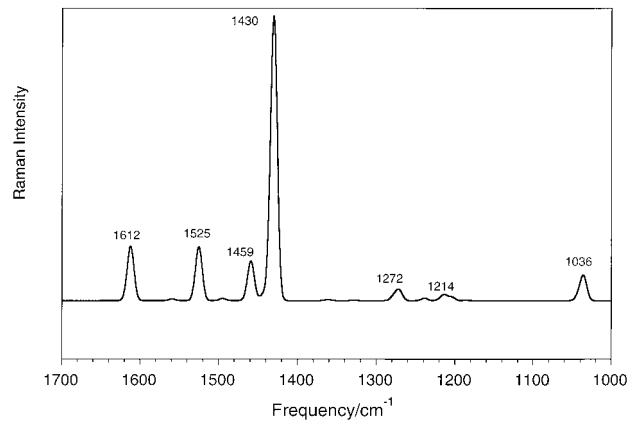

Figure 4. B3P86/6-31G** Raman spectrum calculated for T3VT3. Wavenumbers (in cm^{-1}) are indicated for the most intense peaks.

within parentheses in the following discussion. As mentioned above, although the B3LYP functional is more widely used in the literature, the B3P86 functional provides more accurate geometries for sulfur-containing conjugated compounds and the force field calculated using this functional is therefore expected to be more accurate.

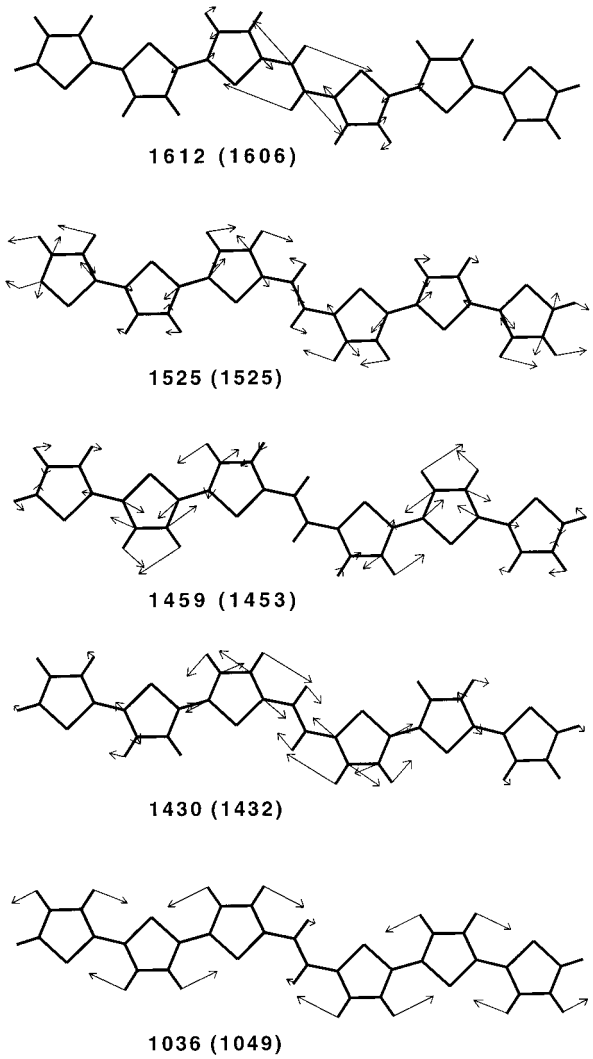

Figure 5. Schematic eigenvectors for the most intense Raman-active symmetric vibrations of T3VT3 calculated at the B3P86/6-31G** level. Scaled and experimental (within parentheses) wavenumbers are given in cm^{-1}.

The Raman line observed at 1606 cm^{-1} is calculated at 1612 cm^{-1} (B3LYP, 1597 cm^{-1}) and is characteristic of the vinylene spacer. As Figure 5 shows, it almost purely corresponds to the C═C stretching of the vinylene group. This vibration is recorded at 1601 cm^{-1} in T2VT2[27] and, as expected, is absent in the spectra of α,α′-dimethyloligothiophenes.[54] The ν(C═C) vinylene vibration upshifts by 5 cm^{-1} in going from T2VT2 to T3VT3 but undergoes a sizable downshift in frequency with respect to TVT (1618 cm^{-1}).[29] Theoretical calculations predict a continuous downshift from TVT (B3P86, 1631 cm^{-1}; B3LYP, 1616 cm^{-1}) to T2VT2 (B3P86, 1615 cm^{-1}; B3LYP, 1600 cm^{-1}) and to T3VT3 (B3P86, 1612 cm^{-1}; B3LYP, 1597 cm^{-1}). This downshift is evidence that the vinylene group is actively involved in the conjugation path and that oligothiophene units longer than the trimer will still slightly affect the properties of the spacer.

The band at 1296 cm^{-1} correlates with the band calculated at 1272 cm^{-1} (B3LYP, 1279 cm^{-1}) and is also characteristic of the vinylene group. It is associated with the in-plane symmetric bending mode of the C—H bonds attached to the spacer. This band appears at the same frequency for T2VT2.

The band recorded at 1525 cm^{-1} was observed at 1539 cm^{-1}

for T2VT2, for which it was correlated with the usually termed line A of α,α′-dimethyloligothiophenes. The band is calculated at 1525 cm^{-1} (B3LYP, 1514 cm^{-1}) and its eigenvector (Figure 5) indicates an in-phase antisymmetric ν_{as}(C═C) vibration of the innermost and outermost thiophene rings of T3VT3; i.e., it is mainly located on the rings at both ends of each terthiophene unit. This displacement pattern agrees with that calculated for line A. For α,α′-dimethyloligothiophenes, line A downshifts by 13 cm^{-1} between the trimer and tetramer and by 8 cm^{-1} from the tetramer to the pentamer and enhances its intensity as the oligomer lengthens.[54] A similar downshift of 14 cm^{-1} and increase of intensity is observed in passing from T2VT2 to T3VT3 (see Figure 3). The similar behavior found for both oligomer series suggests that this vibration is strongly located on the oligothiophene moieties in agreement with the calculated eigenvector. On the other hand, the frequency recorded for T3VT3 (1525 cm^{-1}) is identical to that of the pentamer (DMqT), indicating that there is an effective electron delocalization between the terthiophene moieties.

The strongest Raman band of T3VT3 appears at 1432 cm^{-1}, almost exactly matching the frequency recorded for T2VT2 (1433 cm^{-1}).[27] T3VT3 furthermore presents a very intense peak at higher frequencies (1453 cm^{-1}), which is completely absent for T2VT2. For this molecule, the band at 1433 cm^{-1} was tentatively assigned to the so-called line B of α,α′-dimethyloligothiophenes, which appears about 1480 cm^{-1} (Table 1) and is always the most intense line of the spectrum.[54] The theoretical vibration associated with line B in α,α′-oligothiophenes describes an in-phase symmetric ν_s(C═C) vibration spreading over the whole molecule. This normal mode corresponds to the collective in-phase oscillation of all the alternating C═C/C—C bonds forming the conjugation path and is chosen as the ECC mode used to estimate the conjugation length.[54] The double-peak structure observed for T3VT3 is not found for α,α′-oligothiophenes.

As can be seen in Figure 4, DFT calculations predict the double-peak structure observed experimentally for T3VT3 in the 1400−1500 cm^{-1} spectral region, although the relative intensities of the peaks are not well reproduced. At the B3P86 level, the most intense peak is calculated at 1430 cm^{-1} (B3LYP, 1411 cm^{-1}) in good agreement with the experiment (1432 cm^{-1}). The eigenvector for this mode describes a symmetric ν_s(C═C) vibration mainly located on the thiophene rings directly linked to the vinylene spacer with a small in-phase oscillation of the neighboring rings (see Figure 5). The stretching of the CC bonds is coupled with the in-phase bending of the C—H bonds in which the H atoms move with a large displacement which opposes that of the C atoms. The lower intensity peak is calculated at 1459 cm^{-1} (B3LYP, 1443 cm^{-1}), and the vibrational mode eigenvector shows the same displacement pattern discussed for the previous mode but now is mostly located on the central thiophene rings (see Figure 5). A third mode with identical characteristics but mainly located on the outer thiophene rings is calculated at 1443 cm^{-1} (B3LYP, 1428 cm^{-1}). The low intensity of this mode precludes its observation in the spectrum.

DFT calculations therefore predict the existence of three Raman-active normal modes in the region 1450−1400 cm^{-1} associated with the ν_s(C═C) vibrations of the three different types of thiophene rings of T3VT3. For all three vibrations, the mechanical coupling between neighboring rings is quite small; no in-phase C═C motion spreading over the whole molecule, similar to the line B in α,α′-dimethyloligothiophenes,[54] is calculated for T3VT3. The theoretical description for the most intense region of the Raman spectrum of T3VT3 thus differs from that of α,α′-oligothiophenes. The difference is due to the vinylene spacer. The vinylene C1—C1′ bond is significantly shorter than the CC double bonds of the thiophene rings and its vibration at about 1600 cm^{-1} is well isolated from the rest of the chain. The C1—C1′ bond shows almost no contribution to the vibrational modes associated with the C═C stretchings of the oligothienylene units, thus breaking in some degree the coupling between these lateral units.

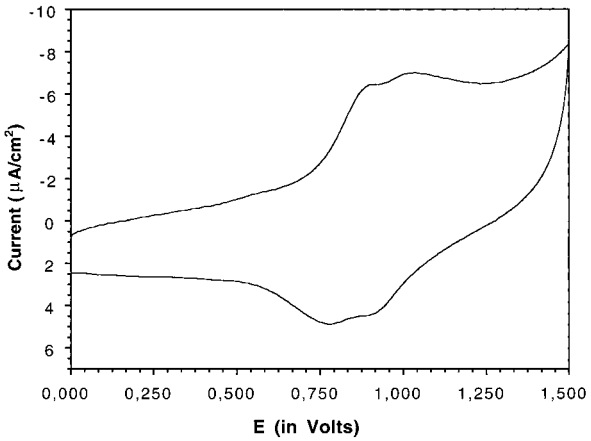

Figure 6. Cyclic voltammogram of T3VT3 in 0.1 M $TBABF_4/CH_2Cl_2$: scan rate 250 mV s^{-1}, reference Ag/AgCl. Scan is initiated in the positive direction.

α,α′-Oligothiophenes also present the so-called line D around 1050 cm^{-1}. This line has a medium intensity and corresponds to the in-phase symmetric bending mode of the C—H bonds attached to the *β*-positions of the thiophene rings. For the T3VT3 cooligomer, this characteristic band is measured at 1049 cm^{-1} and is calculated at 1036 cm^{-1} (B3LYP, 1036 cm^{-1}). The band actually involves two vibrations, the most intense of which corresponds to the totally in-phase oscillation depicted in Figure 5. Theoretical calculations also predict a weak band at 1214 cm^{-1} (B3LYP, 1195 cm^{-1}) that correlates with the experimental band observed at 1225 cm^{-1}. This band mainly defines the ν(C—C) vibration of the C1—C2 bonds linking the terthiophene units to the vinylene spacer.

It should be mentioned that the Raman spectrum was also calculated for two other conformations of T3VT3: the most stable twisted-form of conformation A and conformation B. In the first case, the spectrum obtained is identical to that plotted in Figure 4, thus proving the reliability of assuming a planar C_{2h} structure. In the second case, the spectrum is also very similar but the vibrations associated with the bands observed in the 1300−1200 cm^{-1} range are calculated at higher energies, suggesting that conformation B does not actually contribute to the experimental spectrum.

IV. Doped T3VT3

(a) Cyclic Voltammetry. Figure 6 shows the cyclic voltammogram recorded for a saturated dichloromethane T3VT3 solution containing 0.1 M $TBABF_4$ at a scan rate of 250 mV/s. The CV exhibits two close one-electron oxidation processes at 0.88 and 1.01 V. The coupled reduction processes appear at 0.77 and 0.90 V, respectively. The two processes are reversible and the CV is reproducible during multiple cycles, showing that no polymerization or degradation processes take place.

No electrochemical study has been previously reported for T_nVT_n cooligomers, but Roncali et al. have studied the electrochemical properties of various *n*TV series using cyclic

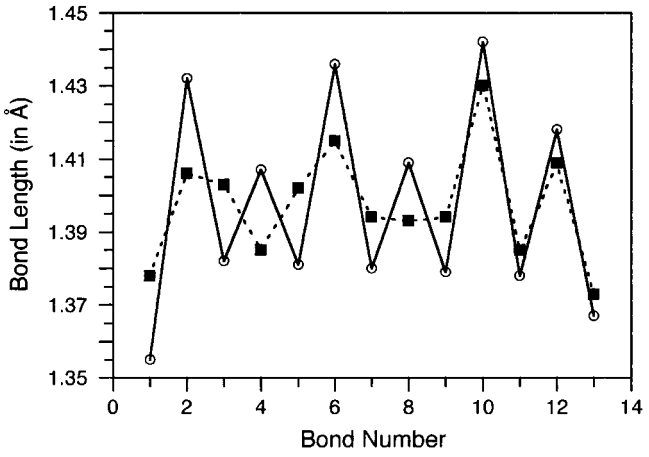

Figure 7. Optimized bond lengths calculated for half the CC path of neutral T3VT3 (open circles) at the B3P86/6-31G** level and for $T3VT3^{\bullet+}$ (filled squares) at the UB3P86/6-31G** level. The bond numbering is from the center toward one end of the oligomer, bond number 1 corresponding to the vinylene C1−C1′ bond.

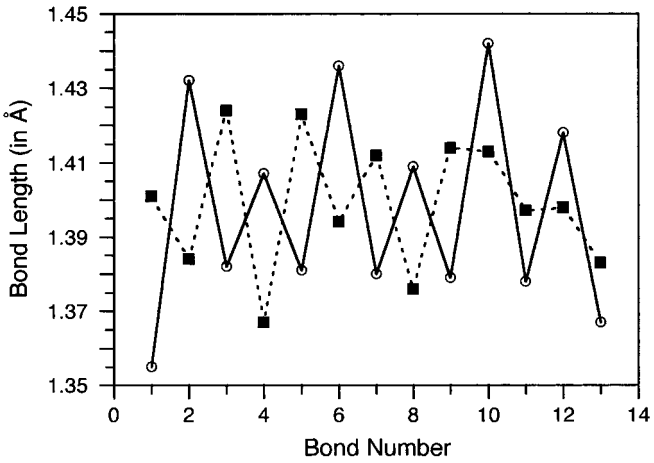

Figure 8. Optimized bond lengths calculated for half the CC path of neutral T3VT3 (open circles) and the closed-sell dication $T3VT3^{2+}$ (filled squares) at the B3P86/6-31G** level. The bond numbering is from the center toward one end of the oligomer, bond number 1 corresponding to the vinylene C1−C1′ bond.

voltammetry.[8,55−57] These authors observed that the CV of the TVT cooligomer displays an irreversible first oxidation process due to follow-up polymerization stages.[58] For the tetramers (TVTVTVT), two oxidation processes become reversible, and for the hexamers, the two oxidation peaks almost merge into a single process followed by a third reversible process corresponding to the formation of the trication radical. On the basis of these data, it can be suggested that the two oxidation processes observed for T3VT3 correspond to the initial generation of the radical cation and, after a second electron extraction, to the generation of the dication species. The potential difference between the two oxidation processes (0.13 eV) is intermediate between those observed for *n*TV tetramers (≈0.20 V)[57] and *n*TV hexamers (=0.10 V).[55,56] This result is consistent with the number of conjugated carbon atoms in T3VT3 (26 carbons) that is between the tetramers (22 carbons) and the hexamers (34 carbons).

(b) Equilibrium Structures. The molecular structures of the radical cation and dication of T3VT3 were optimized by keeping planar the molecules in the C_{2h} conformation depicted in Figure 1a (conformation A). As the B3P86 and B3LYP calculations lead to identical trends for both the cation and the dication, only the results obtained at the B3P86/6-31G** level are discussed below.

Figure 7 compares the UB3P86/6-31G** optimized bond lengths calculated for the radical cation of T3VT3 along the CC path with those obtained for neutral T3VT3 at the B3P86/6-31G** level. Oxidation mainly affects the central part of the molecule; the amplitude of the structural modifications progressively decreases from the center to the ends of the cooligomer. The double bond of the vinylene bridge lengthens from 1.355 to 1.378 Å while its two single bonds shorten from 1.432 to 1.406 Å in passing from the neutral form to the radical cation. The thiophene rings directly attached to the vinylene bridge are the most affected by the oxidation and undergo a reversal of the single−double CC bond alternation pattern, reaching a heteroquinonoid structure for $T3VT3^{\bullet+}$. The magnitude of the quinonoid-like bond length alternation for these rings is only 0.017 Å. The central rings of the terthienylene units show no CC bond alternation for $T3VT3^{\bullet+}$. The outermost thiophene rings are slightly affected by the oxidation and preserve a heteroaromatic structure in the radical cation similar to that of the neutral form. The C−S bond lengths remain unchanged upon oxidation, the maximum modification being of 0.008 Å for the terminal C13−S16 bonds.

The equilibrium structure calculated for $T3VT3^{\bullet+}$ indicates the formation of a positive polaron-type defect centered over the vinylene spacer and extending over the two closest thiophene rings. However, the Mulliken atomic charges calculated for T3VT3 and $T3VT3^{\bullet+}$ suggest that the excess of positive charge is evenly distributed over the whole molecule. The electrons extracted per thiophene ring from the center to the ends of $T3VT3^{\bullet+}$ are 0.17e, 0.14e, and 0.16e, respectively.

Closed-shell bipolaron defects are usually invoked to explain the electronic properties of conjugated polymers in their dication state. Van Haare et al. have, however, demonstrated the occurrence of two polarons instead of a bipolaron for long oligothiophenes.[25] We have considered this possibility for T3VT3 by calculating its dication in different electronic configurations using the DFT method. The bipolaron was calculated as a closed-shell dication (^1A_g state). The coexistence of two polarons on the oligomer implies a biradical dication and was calculated as a triplet state (^3B_u) using the spin-unrestricted approximation.[59]

Figure 8 compares the optimized CC bond lengths calculated for the closed-shell dication of T3VT3 with the corresponding values of the neutral molecule. As expected, the structural changes are larger than those obtained for the radical cation. The vinylene C1−C1′ bond (1.401 Å) is now longer that the adjacent C1−C2 bonds (1.384 Å), and both the innermost and the central rings of the terthiophene units present a heteroquinonoid structure. The outermost rings present almost no CC bond length alternation. These structural changes indicate the formation of a positive bipolaron defect (the two charges are associated to a strong quinonoid deformation centered in the middle of the molecule), which extends over the whole molecule. For the biradical dication, the optimized lengths of the C1−C1′ (1.362 Å) and C1−C2 (1.428 Å) bonds are similar to those obtained for neutral T3VT3, and the terthiophene units present a quinonoid structure centered in the central ring. This structure is consistent with the formation of two positive polarons in which the charges are mainly extracted from the terthienylene moieties.

At the B3P86/6-31G** level, the closed-shell dication (the bipolaron) is calculated to be more stable than the biradical dication (two individual polarons) by 6.23 kcal/mol (B3LYP:

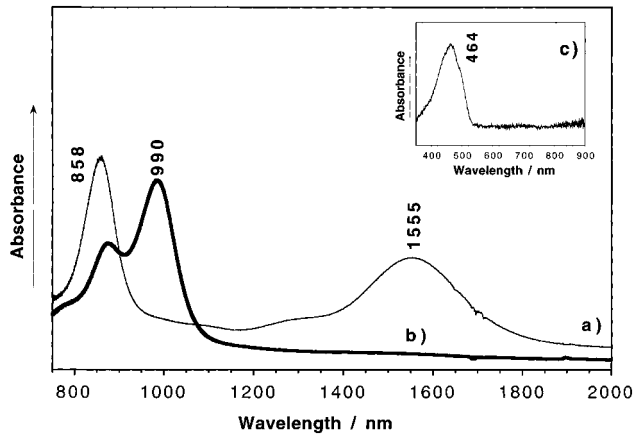

Figure 9. Electronic spectra recorded in dichloromethane for (a) low oxidized species of T3VT3 (obtained after oxidation with trifluoracetic acid), (b) high oxidized species of T3VT3 (obtained after oxidation with ferric chloride), and (c) neutral species.

6.54 kcal/mol). This result shows that the decrease in coulomb repulsion energy obtained by moving the two charges apart in $T3VT3^{2+}$ is not enough to outweigh the energy cost that results from the fact that the two charges no longer share the same geometrical deformation. A closed-shell bipolaron structure is therefore proposed for the ground state of $T3VT3^{2+}$.

(c) UV−Vis−NIR Spectra. The electronic spectra for the radical cation species was obtained after chemical oxidation with trifluoroacetic acid (Figure 9). The first oxidation process is complete within minutes. However, no further oxidation of the molecule was observed under these conditions. The UV−vis−NIR spectrum for the lower oxidized state presents two main bands at 858 nm (1.45 eV) and 1555 nm (0.80 eV) with an important shoulder at 1291 nm (0.96 eV).

The bands at 858 and 1555 nm clearly correspond to the radical cation species on the basis of the data reported in the literature for a large number of oligothiophene radical cations.[4,8,22,23,25,57] For instance, van Haare et al.[25] have recently performed a comprehensive study of a didodecylsexithiophene (6T) in neutral, cation, and dication states. Neutral 6T presents a band at 425 nm (2.92 eV) that disappears upon oxidation to the radical cation which exhibits two strong bands at 780 nm (1.59 eV) and 1476 nm (0.84 eV). Similarly, the tetrathienylenevinylene (TVTVTVT ≡ 4TV) cooligomer end-capped with hexyl chains studied by Levillain et al.[57] presents a band at 465 nm (2.67 eV) in the neutral state and two new bands at 860 nm (1.44 eV) and 1480 nm (0.84 eV) in the cation state. The absorption energies of 4TV are almost identical to those found for T3VT3, suggesting that T3VT3 and 4TV have a very similar conjugation length. Both $6T^{\bullet+}$ and $4TV^{\bullet+}$ form π-dimers that are characterized by a weak absorption at 1107 nm (1.12 eV)[25] and 1120 nm (1.10 eV).[57] On this basis, the weak band that $T3VT3^{\bullet+}$ presents at 1291 nm (0.96 eV) is assigned to the formation of π-dimers.

The generation of dication species was accomplished by the addition of ferric chloride. The radical cation species generated initially with this oxidant gave identical spectra to those generated with trifluoroacetic acid. The electronic spectrum for the higher oxidized species displays an intense absorption band at 990 nm (1.25 eV) with a shoulder at 875 nm (1.42 eV), while the absorptions due to the radical cation have disappeared. By analogy with similar data on oligothiophenes,[25] these spectral features are consistent with the formation of a dication species with a bipolaron structure, for which the two absorption bands of the cation are replaced by a strong absorption at intermediate

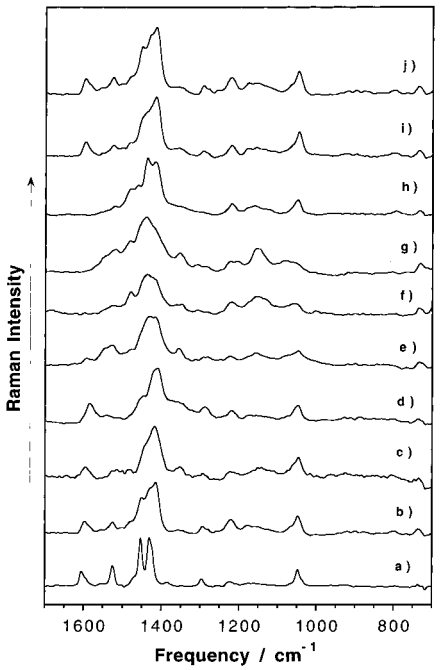

Figure 10. Raman spectra recorded in solid state after electrochemical oxidation at different oxidation potentials: (a) neutral species, (b) 1.00 V, (c) 1.21 V, (d) iodine-oxidized T2VT2, (e) 1.30 V, (f) 1.40 V, (g) 1.50 V, (h) iodine-oxidized DMQqT, (i) −0.70 V, and (j) −0.50 V.

energies. This is the case for $6T^{2+}$, for which the two bands of $6T^{\bullet+}$ are replaced by a strong band at 1.28 eV with a vibronic shoulder at 1.42 eV. These results support the bipolaron electronic state that theoretical calculations predict for $T3VT3^{2+}$.

The electronic spectrum of $T3VT3^{\bullet+}$ was computed at the UB3P86/6-31G** level using the TDDFT approach. Theoretical calculations predict the occurrence of two intense $1^2A_u \rightarrow {}^2B_g$ electronic transitions at 0.92 ($f = 0.41$) and 1.68 eV ($f = 2.20$). No other dipole-allowed state is found below 2 eV. The calculated spectrum is in good agreement with the two absorption bands observed experimentally at 0.80 and 1.45 eV and supports the idea that the weak absorption at 0.98 eV is not due to $T3VT3^{\bullet+}$ and might be associated to the π-dimer as discussed above. The lowest energy band at 0.80 eV is therefore assigned to the transition to the 1^2B_g state, which mainly corresponds to an electronic excitation from the doubly occupied HOMO-1 (b_g) to the singly occupied HOMO (a_u). The highest energy band at 1.45 eV is attributed to the transition to the 2^2B_g state which mainly results from the HOMO (a_u) → LUMO (b_g) excitation.

The electronic spectrum of $T3VT3^{2+}$ was computed at the B3P86/6-31G** level using the optimized bipolaron structure discussed in Figure 8. Below 2 eV, calculations predict that only the transition to the first excited 1^1B_u state is dipole-allowed. The $1^1A_g \rightarrow 1^1B_u$ transition is very intense ($f = 3.04$) and is calculated at an energy of 1.55 eV intermediate between those obtained for the radical cation in good accord with the experiment. The absorption band at 1.25 eV is therefore assigned as the transition to the 1^1B_u state described by the HOMO (b_g) → LUMO (a_u) excitation. Theoretical calculations also suggest that the shoulder observed at 1.42 eV corresponds to a vibrational component, since the next dipole-allowed transition is found at 2.34 eV and has a very low intensity ($f = 0.005$).

(d) Raman Spectra. Figure 10 shows the Raman spectrum of neutral T3VT3 together with the spectra recorded for T3VT3 oxidized at various anodic potentials. The Raman spectra previously reported for iodine-oxidized T2VT2[28] and iodine-

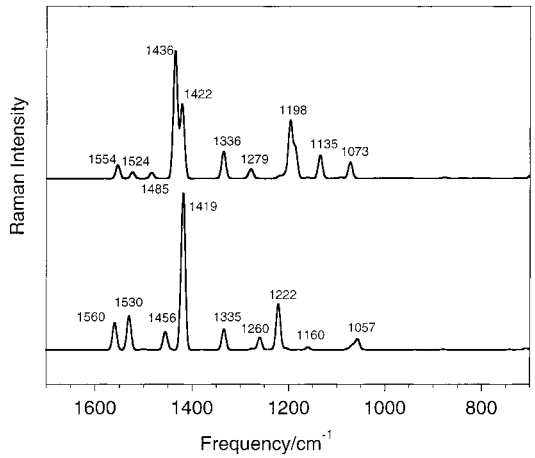

Figure 11. Raman spectra calculated for T3VT3$^{\bullet+}$ (bottom) at the UB3P86/6-31G** level and for T3VT3^{2+} (top) at the B3P86/6-31G** level. Wavenumbers (in cm^{-1}) are indicated for the most intense peaks.

TABLE 2: Correlation between the Vibrational Raman Frequencies Recorded for Neutral T3VT3 and Electrochemically-Doped T3VT3 at Different Anodic Potentials, Together with the Raman Frequencies of Iodine-Doped T2VT2 and DMQqT

T3VT3	1.00 V	1.21 V	T2VT2-I_2[a]	1.30 V	1.40 V	1.50 V	DMQqT-I_2[b]
1606	1598	1597	1585	1593			
1555	1555						
1525	1526			1526			
		1515				1518	1521
		1481			1481	1482	1482
							1461
1453	1451						
1432	1429	sh		1431	1438	1438	1438
1420 sh							
	1417	1417	1410	1418	1418 sh)	1417 sh	1417
1385							
1347		1352		1356	1350	1354	
						1306	
1296	1293	1293	1289	1292			
				1282			
1258	1257						
				1248			
1225	1222	1223	1220	1223	1220	1223	1220
						1207	
1175	1178						
1160				1156	1156	1156	1161
		1151					
1049	1047	1047	1049	1047	1060	1077	1050

[a] From ref 28. [b] From ref 16.

oxidized α,α′-dimethylquinquethiophene[16] are included in Figure 10 for comparison. Table 2 correlates the frequencies measured for the whole series of spectra. Figure 11 displays the Raman spectra calculated for T3VT3$^{\bullet+}$ and T3VT3^{2+} at the UB3P86/ and B3P86/6-31G** levels, respectively. The results obtained using the B3LYP functional are not discussed below because this functional affords the same description of the spectra with small differences for the vibration frequencies. Figure 12 plots the theoretical eigenvectors calculated for selected vibrations of T3VT3$^{\bullet+}$ and T3VT3^{2+}.

(d.1) Low Oxidized Species. In the Raman spectrum recorded after electrochemical oxidation at 1.21 V, the ν(C═C)$_{vinylene}$ band is observed at 1597 cm^{-1}. The frequency of this band decreases with respect to the neutral form by 9 cm^{-1} as a consequence of the gradual loss of double bond character of the vinylenic spacer induced by the quinoidization of the π-conjugated backbone upon oxidation. Theoretical calculations confirm the loss of double bond character of the vinylene spacer, but they predict a larger downshift for the associated vibration

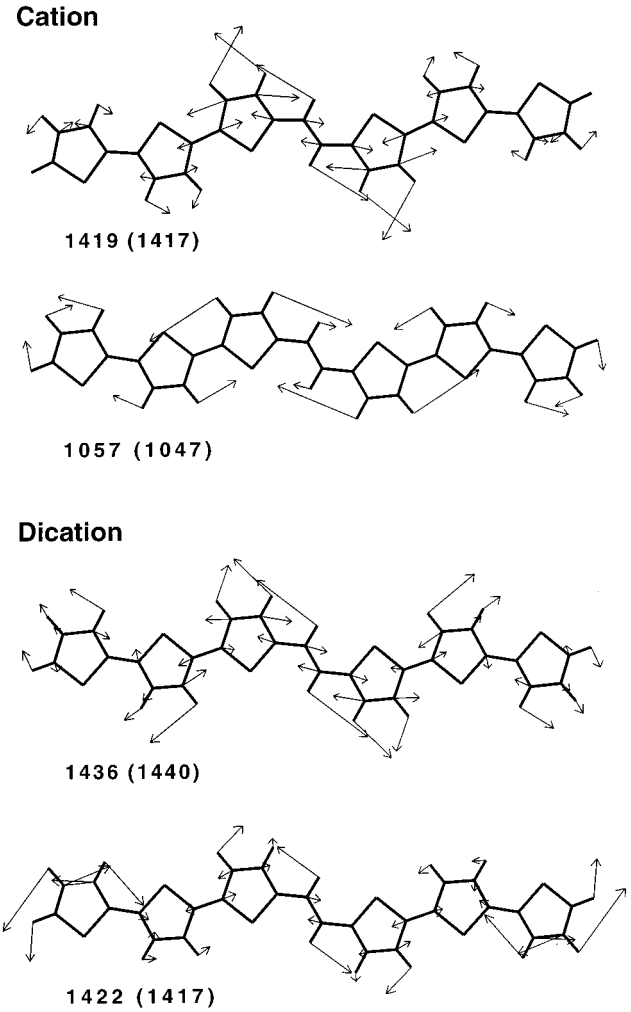

Figure 12. Schematic eigenvectors for selected Raman-active vibrations calculated for T3VT3$^{\bullet+}$ (top) at the UB3P86/6-31G** level and for T3VT3^{2+} (bottom) at the B3P86/6-31G** level. Scaled and experimental (within parentheses) wavenumbers are given in cm^{-1}.

calculated at 1560 cm^{-1} (1612 cm^{-1} for neutral T3VT3). The reason for this shift is that the stretching of the vinylene double bond is now coupled with the C═C stretching of the adjacent rings due to very small bond alternation found along the CC path for T3VT3$^{\bullet+}$ (see Figure 7). This coupling is also found for the quite intense vibration calculated at 1530 cm^{-1} whose eigenvector corresponds to line A; however, this line is very weak in the experimental spectrum.

The most intense scattering in the Raman spectrum of the low oxidized species is a broad band with a maximum at 1417 cm^{-1}. This band correlates with the Raman line at 1432 cm^{-1} in the neutral form of T3VT3. The downshift by 15 cm^{-1} after oxidation is also consistent with the generation of a quinonoid structure upon doping. Calculations predict a downshift of 13 cm^{-1} for the strongest line (1419 cm^{-1}) in good agreement with the experimental value. The associated eigenvector (Figure 12) is mainly located on the central part of the molecule, as it was also the case for the neutral molecule (Figure 5) and implies the in-phase stretching of the β—β and α—α bonds also involving the vinylene bridge. This normal mode defines the stretching of the quinonoid structure associated with the polaron defect. It is clearly related to the vibrational coordinate, which describes the transition from an aromatic to a quinonoid structure. The low intensity peak calculated at 1456 cm^{-1} correlates with the shoulder observed experimentally on the high-frequency side of the main band.

The band at 1352 cm^{-1} grows in intensity upon oxidation and is calculated at 1335 cm^{-1}. It is assigned to a mixed intra- and inter-ring ν(CC) vibration with no contribution of the vinylene spacer. The band at 1293 cm^{-1} (calculated at 1260 cm^{-1}) corresponds, as for neutral T3VT3, to the symmetric bending mode of the vinylene C—H bonds. The bands at 1223 and 1151 cm^{-1} are calculated at 1222 and 1160 cm^{-1} and are assigned to intra-ring ν(CC) vibrations of CC bonds which lose double bond character upon quinoidization of the π-conjugated skeleton. Finally, the band at 1047 cm^{-1} (calculated at 1057 cm^{-1}) corresponds to the symmetric C—H vibration, δ_s(C—H), or line D, as assigned in the neutral molecule, but now the outermost thiophene rings oscillate out-of-phase (see Figure 12) due to the aromatic-type structure of these rings.

A comparison of the Raman spectrum of T3VT3 oxidized at 1.21 V with that of iodine-oxidized T2VT2 (a radical cation species[28]) shows that, in both spectra, the frequency and intensity patterns are almost the same. Small differences of the frequency values appear for the $\nu(C{=}C)_{vinylene}$ vibration and for the most intense band (see Table 2). For T2VT2, both vibrations downshift by 12 and 7 cm^{-1}, respectively. These differences could be due to the larger extension of the quinonoid structure in the case of T3VT3, as theoretical calculations confirm on going from T2VT2 to T3VT3. In combination with electrochemical, optical, and theoretical results, it is concluded that the lower oxidation state in T3VT3 is compatible with the generation of a radical cation species.

(d.2) Highly Oxidized Species. In the Raman spectrum recorded after electrochemical oxidation at 1.50 V, the most intense scattering appears at 1438 cm^{-1} with a shoulder at 1417 cm^{-1}. This band correlates with the Raman line at 1432 cm^{-1} of neutral T3VT3 and with the band at 1417 cm^{-1} of $T3VT3^{\bullet+}$. B3P86 calculations for $T3VT3^{2+}$ predict the most intense band at 1436 cm^{-1} with a shoulder at 1422 cm^{-1} in good agreement with the experiment. The two vibrational modes have an intensity ratio of 2:1 and are depicted in Figure 12. The vibration at 1436 cm^{-1} defines the totally in-phase ν(C=C) stretching of the bipolaronic defect, whose quinonoid structure is more largely extended than in $T3VT3^{\bullet+}$. The vibration at 1422 cm^{-1} is similar but is now mainly located on the outermost thiophene rings that oscillate out-of-phase with respect to the innermost rings due to their intermediate structure with almost no CC bond alternation.

The Raman spectrum shows several weak bands on the high energy side of the main band. Calculations predict three low intensity bands in that region due to vibrations of the CC bonds with more double character oscillating with different phases. On the low energy side a band at 1354 cm^{-1} (calculated at 1336 cm^{-1}) that was already observed for the radical cation is present. The assignment of the vibrational Raman bands of the dication is completed by mentioning the triplet at 1223 (1207), 1156, and 1077 cm^{-1}. Three bands are also calculated in this region at 1198 (1187), 1135 and 1073 cm^{-1}. The first two bands correspond to ring ν(C—C) vibrations involving the C_α—C_β bonds, which now have a more pronounced single-bond character, and also the vinylene C1—C1′ bond. The band at 1073 cm^{-1} corresponds to line D and shows a vibrational pattern almost identical to that depicted in Figure 12 for $T3VT3^{\bullet+}$.

The Raman spectra of T3VT3 as a function of the electrochemical doping level show an interesting behavior. In α,α′-dimethyl oligothiophenes, the most intense Raman bands (associated with the ECC mode) always downshift from the neutral to the radical cation and, finally, to the dication species (e.g., for α,α′-dimethylquinquethiophene, from 1477 to 1438 cm^{-1} and to 1415 cm^{-1}). For T3VT3, the most intense band downshifts from 1432 cm^{-1} in the neutral species to 1417 cm^{-1} in the radical cation, but it upshifts to 1438 cm^{-1} in the dication. This difference in behavior is also predicted by theoretical calculations and is due to the vinylene spacer, which shows a CC bond length alternation smaller than the thiophene rings for $T3VT3^{2+}$. This confirms that Raman spectroscopy is a very sensitive tool to analyze the quinonoid structures generated after doping in conjugated molecules.

V. Conclusions

The vibrational and electronic properties of a novel well—barrier—well vinylene-bridged sexithiophene oligomer (T3VT3) have been investigated in both neutral and oxidized states by using FT-Raman and UV—vis—NIR spectroscopies together with DFT theoretical calculations. Comparison with data for other linear thiophene-based oligomers shows that the presence of the vinylene bridge strongly influences those properties.

Neutral T3VT3 is predicted to have a nearly planar all-anti structure and presents an intense optical absorption at 464 nm, which has been assigned to the HOMO → LUMO ($1^1A_g \rightarrow 1^1B_u$) electronic transition. This absorption is bathochromically shifted with respect to that observed for sexithiophene (425 nm)[25] showing that the effective conjugation length of T3VT3 surpasses that of 6T. The enhancement of the conjugation length has been also observed for thienylenevinylene oligomers (*n*TVs) by Roncali et al.[8,55,56] T3VT3 presents in fact a conjugation length similar to 4TV.

The Raman spectrum of T3VT3 has been comprehensively assigned on the basis of theoretical calculations and presents the following characteristics: (i) the vibrations of the vinylene group appear clearly differentiated from the vibrations of the rest of the chain; (ii) it preserves some of the vibrational features typically observed for α,α′-oligothiophenes, such as the so-called A and D lines; (iii) the most intense band exhibits a double-peak structure in contrast to the single-peak observed for α,α′-oligothiophenes; and (iv) no collective in-phase oscillation of all the CC bonds forming the conjugation path, similar to the ECC mode giving rise to line B in α,α′-oligothiophenes, is calculated for T3VT3. The reason for these vibrational characteristics is that the vinylene spacer breaks in some degree the coupling between the lateral terthiophene units. The vinylenic C1—C1′ bond is significantly shorter than the double CC bonds of the thiophene rings and contributes very little to the C=C stretchings of the terthiophene units.

T3VT3 presents two reversible oxidation processes that have been assigned to the formation of the radical cation and dication, respectively. The equilibrium structure calculated for $T3VT3^{\bullet+}$ indicates the formation of a positive polaron-type defect centered over the vinylene spacer and extending over the two closest thiophene rings. For $T3VT3^{2+}$, theoretical calculations predict the formation of a bipolaron defect, in which the two charges are associated with a strong quinonoid deformation centered in the middle of the molecule and extending over the whole molecule. The optical features observed in the UV—vis—NIR spectra are consistent with the formation of a polaron defect for $T3VT3^{\bullet+}$ and a closed-shell bipolaron defect for $T3VT3^{2+}$.

The evolution of the Raman spectra with the doping level also evidences the formation of a quinonoid structure for $T3VT3^{\bullet+}$ and $T3VT3^{2+}$. The most intense Raman band is due to a C=C stretching normal mode of the polaron/bipolaron defect, which defines the vibrational coordinate associated with the transition from an aromatic to a quinonoid structure. The vinylene spacer determines that this Raman band does not

progressively downshift upon increasing oxidation, as observed for the nonintercalated α,α′-oligothiophenes.

To our knowledge, this work constitutes the first attempt to combine DFT theoretical calculations with experimental UV−vis−NIR and Raman data, on both neutral and doped species, to gain an overall insight into the structures of different types of charge defects in the class of π-conjugated materials.

Acknowledgment. The present work was supported in part by the Dirección General de Enseñanza Superior (DGES, MEC, Spain) through the research projects BQU2000-1156, PB98-1447, and 1FD97-1765-C03. We are also indebted to the Junta de Andalucía (Spain) for funding our research group (FQM-0159). J.C. is grateful to the Ministerio de Educacion y Cultura of Spain for a postdoctoral fellowship (Formación y Perfeccionamiento de Doctores y Tecnólogos en el Extranjero, ref PF00 25327895). K.R.M. acknowledges the National Science Foundation under grant No. CHE-9307837.

References and Notes

(1) Elsenbaumer, R. L.; Skotheim, T.; Reynolds, J. R. *Handbook of Conductive Polymers*; Dekker: New York, 1998.

(2) Müllen, K.; Wegner, G. *Electronic Materials: The Oligomer Approach*; Wiley-VCH: Weinheim, 1998.

(3) Martin, R. E.; Diederich, F. *Angew. Chem., Int. Ed. Engl.* **1999**, *38*, 1350.

(4) Miller, L. L.; Mann K. R. *Acc. Chem. Res.* **1996**, *29*, 417.

(5) Cournil, J.; dos Santos, D. A.; Crispin, X.; Silbey, R.; Brédas, J. L. *J. Am. Chem. Soc.* **1998**, *120*, 1289.

(6) Yang, S. C.; Graupner, W.; Guha, S.; Puschnig, P.; Martin. C.; Chandrasekhar, H. R.; Chandrasekhar, M.; Leising, G.; Ambrosch-Draxl, C.; Scherf, U. *Phys. Rev. Lett.* **2000**, *85*, 2388.

(7) Tour, J. M. *Chem. Rev.* **1996**, *96*, 537.

(8) Roncali, J. *Acc. Chem. Res.* **2000**, *33*, 147.

(9) Fichou, D. *Handbook of Oligo- and Polythiophenes*; Wiley-VCH: Weinheim, 1999.

(10) Garnier, F. *Acc. Chem. Res.* **1999**, *32*, 209.

(11) Garnier, F.; Hajlaoui, R.; Yassar, A.; Srivastava, P. *Science* **1994**, *265*, 1684. Dodabalapur, A.; Katz, H. E.; Torsi, L.; Haddon, R. C. *Science* **1995**, *269*, 1560.

(12) Roncali, J. *Chem. Rev.* **1997**, *97*, 173.

(13) Brédas, J. L. *J. Chem. Phys.* **1985**, *82*, 3808.

(14) Sakamoto, A.; Furukawa, Y.; Tasumi, M. *J. Phys. Chem.* **1994**, *98*, 4635.

(15) Yokonuma, N.; Furukawa, Y.; Tasumi, M.; Kuroda, M.; Nakayama, J. *Chem. Phys. Lett.* **1996**, *255*, 431.

(16) Casado, J.; Hernández, V.; Hotta, S.; López Navarrete, J. T. *J. Chem. Phys.* **1998**, *109*, 10419.

(17) Casado, J.; Hernández, V.; Hotta, S.; López Navarrete, J. T. *Adv. Mater.***1998**, *10*, 1258; Casado, J.; Hernández, V.; Ramírez, F. J.; Hotta, S.; López Navarrete, J. T. *Opt. Mater.* **1998**, *9*, 82.

(18) Castiglioni, C.; Gussoni, M.; López Navarrete, J. T.; Zerbi, G. *Solid State Commun.* **1988**, *65*, 625. López Navarrete, J. T.; Zerbi, G. *J. Chem. Phys.* **1991**, *94*, 957 and 965.

(19) Hernández, V.; Castiglioni, C.; del Zoppo, M.; Zerbi, G. *Phys. Rev. B* **1994**, *50*, 9815.

(20) Ehrendorfer, Ch.; Karpfen, A. *J. Phys. Chem.* **1994**, *98*, 7492.

(21) Hill, M. G.; Mann, K. R.; Miller, L. L.; Penneau, J. F. *J. Am. Chem. Soc.* **1992**, *114*, 2728; Zinger, B.; Mann, K. R.; Hill, M. G.; Miller, L. L. *Chem. Mater.* **1992**, *4*, 1113.

(22) Bauerle, P.; Segelbacher, U.; Maier, A.; Mehring, M. *J. Am. Chem. Soc.* **1993**, *115*, 10217.

(23) Zotti, G.; Schiavon, G.; Berlin, A.; Pagani, G. *Chem. Mat.* **1993**, *5*, 620.

(24) Hicks, R. G.; Nodwell, M. B. *J. Am. Chem. Soc.* **2000**, *122*, 6746.

(25) van Haare, J. A. E. H.; Havinga, E. E.; van Dogen, J. L. J.; Janssen, R. A. J.; Cornil, J.; Brédas, J. L. *Chem. Eur. J.* **1998**, *4*, 1509.

(26) Tol, A. J. W. *Chem. Phys.* **1996**, *208*, 73. Tol, A. J. W. *Synth. Met.* **1995**, *74*, 95.

(27) Hernández, V.; Casado, J.; Kanemitsu, Y.; López Navarrete, J. T. *J. Chem. Phys.* **1999**, *110*, 6907.

(28) Casado, J.; Hernández, V.; Kanemitsu, Y.; López Navarrete, J. T. *J. Raman Spectrosc.* **2000**, *31*, 565.

(29) Louarn, G.; Mévellec, J. Y.; Lefrant, S.; Buisson, J. P.; Fichou, D.; Teulade-Fichou, M. P. *Synth. Met.* **1995**, *69*, 351.

(30) Kanemitsu, Y.; Suzuki, Y.; Matsumoto, Y.; Tomiuchi, Y.; Shiraishai, Y.; Kuroda, M. *Phys. Rev. B* **1994**, *50*, 2301.

(31) Zinger, B.; Mann, K. R.; Hill, M. G.; Miller, L. L. *Chem. Mater.* **1992**, *4*, 1113.

(32) Frisch, M. J.; Trucks, G. W.; Schlegel, H. B.; Scuseria, G. E.; Robb, M. A.; Cheeseman, J. R.; Zakrzewski, V. G.; Montgomery, J. A.; Stratman, R. E.; Burant, J. C.; Dapprich, S., Millam, J. M.; Daniels, A. D.; Kudin, K. N.; Strain, M. C.; Farkas, O.; Tomasi, J.; Barone, V.; Cossi, M.; Cammi, R.; Mennucci, B.; Pomelli, C.; Adamo, C.; Clifford, S.; Ochterski, J.; Petersson, G. A.; Ayala, P. Y.; Cui, Q.; Morokuma, K.; Malick, D. K.; Rabuck, A. D.; Raghavachari, K.; Foresman, J. B.; Cioslowski, J.; Ortiz, J. V.; Baboul, A. G.; Stefanov, B. B.; Liu, G.; Liashenko, A.; Piskorz, P.; Komaromi, I.; Gomperts, R.; Martin, R. L.; Fox, D. J.; Keith, T.; Al-Laham, M. A.; Peng, C. Y.; Nanayakkara, A.; Gonzalez, C.; Challacombe, M.; Gill, P. M. W.; Johnson, B.; Chen, W.; Wong, M. W.; Andres, J. L.; Head-Gordon, M.; Replogle, E. S.; Pople, J. A. *Gaussian 98*, Revision A.7; Gaussian, Inc.: Pittsburgh, PA, 1998.

(33) Perdew, J. P. *Phys. Rev. B* **1986**, *33*, 8822.

(34) Becke, A. D. *J. Chem. Phys.* **1993**, *98*, 1372.

(35) Francl, M. M.; Pietro, W. J.; Hehre, W. J.; Binkley, J. S.; Gordon, M. S.; Defrees, D. J.; Pople, J. A. *J. Chem. Phys.* **1982**, *77*, 3654.

(36) Viruela, P. M.; Viruela, R.; Ortí, E.; Brédas, J.-L. *J. Am. Chem. Soc.* **1997**, *119*, 1360.

(37) Liu, R.; Zhou, X.; Kasmai, H. *Spectrochim. Acta A* **1997**, *53*, 1241.

(38) Altmann, J. A.; Handy, N. C.; Ingamells, V. E. *Mol. Phys.* **1997**, *92*, 339.

(39) Scott, A. P.; Radom, L. *J. Phys. Chem.* **1996**, *100*, 16502.

(40) Runge, E.; Gross, E. K. U. *Phys. Rev. Lett.* **1984**, *52*, 997.

(41) Gross, E. K. U.; Kohn, W. *Adv. Quantum Chem.* **1990**, *21*, 255.

(42) Gross, E. K. U.; Ullrich, C. A.; Gossmann, U. J. In *Density Functional Theory*; Gross, E. K. U., Driezler, R. M., Eds.; Plenum Press: New York, 1995; p 149.

(43) Casida, M. E. In *Recent Advances in Density Functional Methods, Part I*; Chong, D. P., Ed.; World Scientific: Singapore, 1995; p 155.

(44) Wiberg, K. B.; Stratmann, R. E.; Frisch, M. J. *Chem. Phys. Lett.* **1998**, *297*, 60. Stratmann, R. E.; Scuseria, G. E.; Frisch, M. J. *J. Chem. Phys.* **1998**, *109*, 8218.

(45) Hsu, C.-P.; Hirata, S.; Head-Gordon, M. *J. Phys. Chem. A* **2001**, *105*, 451.

(46) Hirata, S.; Lee, T. J.; Head-Gordon, M. *J. Chem. Phys.* **1999**, *111*, 8904.

(47) Koch, W.; Holthausen, M. C. *A Chemist's Guide to Density Functional Theory*; Wiley-VCH: Weinheim, 2000.

(48) Krishnan, R.; Binkley, J. S.; Seeger, R.; Pople, J. A. *J. Chem. Phys.* **1980**, *72*, 650.

(49) Viruela, P. M.; Viruela, R.; Ortí, E. *Int. J. Quantum Chem.* **1998**, *70*, 303.

(50) Karpfen, A.; Choi, C. H.; Kertesz, M. *J. Phys. Chem. A* **1997**, *101*, 7426.

(51) Porzio, W.; Destri, S.; Mascherpa, M.; Brückner, S. *Acta Polym.* **1993**, *44*, 266. Horowitz, G.; Bachet, B.; Yassar, A.; Lang, P.; Demanze, F.; Fave, J. L. Garnier, F. *Chem. Mater.* **1995**, *7*, 1337.

(52) Serrano-Andrés, L.; Merchán, M.; Nebot-Gil, I.; Lindh, R.; Roos, B. O. *J. Chem. Phys.* **1993**, *98*, 3151.

(53) Serrano-Andrés, L.; Lindh, R.; Roos, B. O.; Merchán, M. *J. Phys. Chem.* **1993**, *97*, 9360.

(54) Hernández, V.; Casado, J.; Ramírez, F. J.; Zotti, G.; Hotta, S.; López Navarrete, J. T. *J. Chem. Phys.* **1996**, *104*, 9271.

(55) Elandaloussi, E.; Frère, P.; Richomme, P.; Orduna, J.; Garín, J.; Roncali, J. *J. Am. Chem. Soc.* **1997**, *119*, 10774.

(56) Jestin, I.; Frère, P.; Mercier, N.; Levillain, E.; Stievenard, D.; Roncali, J.. *J. Am. Chem. Soc.* **1998**, *120*, 8150.

(57) Levillain, E.; Roncali, J. *J. Am. Chem. Soc.* **1999**, *121*, 8760.

(58) Roncali, J.; Thobie-Gautier, C.; Elandaloussi, E.; Frère, P. *J. Chem. Soc., Chem. Commun.* **1994**, 2249.

(59) The biradical dication was also computed as a singlet state (^1A_g) within the spin-unrestricted approach using the mixed-spin state option (GUESS=MIX) of Gaussian 98. This option builds, as the initial guess wave function, a 1:1 mixture of the singlet and triplet states with a spin-squared expectation value $\langle S^2 \rangle = 1$ and has been shown to provide reliable geometries and energies for singlet-state biradicals even though the spin density it provides is fully wrong (Davidson, E. R. *Int. J. Quantum Chem.* **1998**, *69*, 241. Lahti, P. M.; Ichimura, A. S.; Sanborn, J. A. *J. Phys. Chem. A* **2001**, *105*, 251). In the case of $T3VT3^{2+}$, both the UB3P86/ and the UB3LYP/GUESS=MIX calculations of the singlet-state biradical converged to the closed-shell ^1A_g state.